LASER INTERFEROMETER GRAVITATIONAL WAVE OBSERVATORY
- LIGO -
CALIFORNIA INSTITUTE OF TECHNOLOGY
MASSACHUSETTS INSTITUTE OF TECHNOLOGY

Technical Note	**LIGO-T22xxxxx–**	2023/08/08

Sensor Fusion for Improved Length Sensing and Control: Report 2

Deven Bowman

California Institute of Technology
LIGO Project, MS 18-34
Pasadena, CA 91125
Phone (626) 395-2129
Fax (626) 304-9834
E-mail: info@ligo.caltech.edu

Massachusetts Institute of Technology
LIGO Project, Room NW22-295
Cambridge, MA 02139
Phone (617) 253-4824
Fax (617) 253-7014
E-mail: info@ligo.mit.edu

LIGO Hanford Observatory
Route 10, Mile Marker 2
Richland, WA 99352
Phone (509) 372-8106
Fax (509) 372-8137
E-mail: info@ligo.caltech.edu

LIGO Livingston Observatory
19100 LIGO Lane
Livingston, LA 70754
Phone (225) 686-3100
Fax (225) 686-7189
E-mail: info@ligo.caltech.edu

http://www.ligo.caltech.edu/

Contents

1 Introduction

Gravitational waves are distortions in spacetime produced by accelerating masses. Their existence was predicted over 100 years ago with the development of general relativity and the first experimental observation was made on September 14, 2015 by the Laser Interferometer Gravitational Wave Observatory (LIGO) and Virgo collaborations of gravitational waves produced by a merger of 2 black holes.[1].

The Advanced LIGO detector is a pair of Michelson interferometers in Washington State and Louisiana with 4km arms [4]. The detector design includes several optical cavities to increase sensitivity. These include Faby-Perot cavities in each arm, a power recycling cavity, and a signal recycling cavity. A diagram of the interferometer is shown in figure 1.

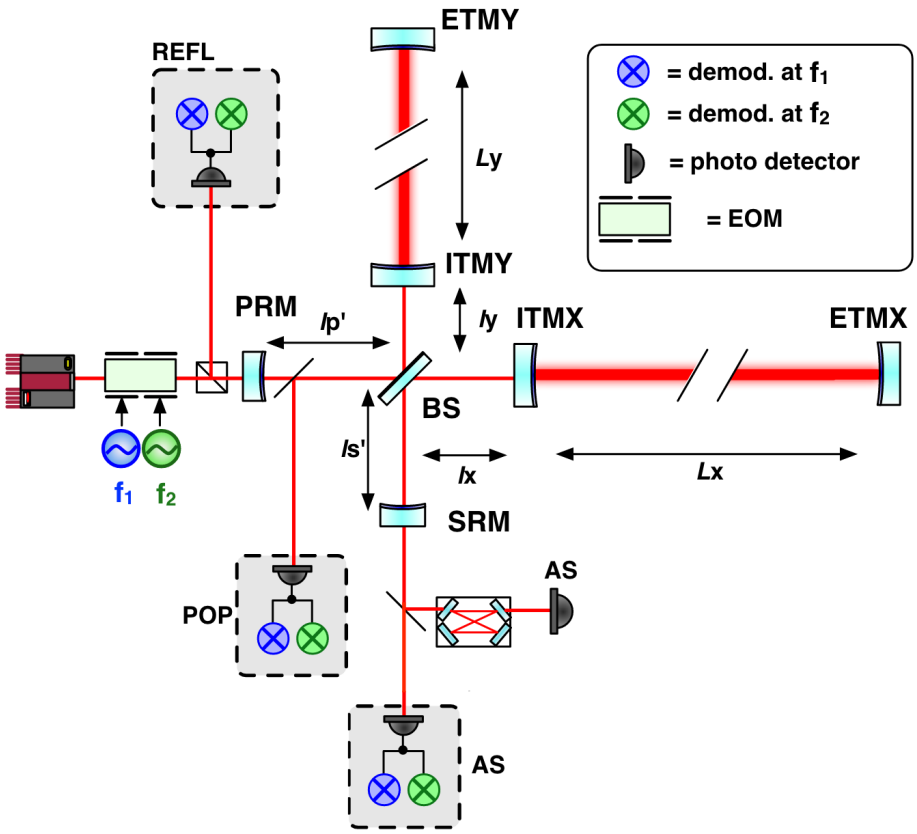

Figure 1: A diagram of one of the Advanced LIGO detectors [8]. REFL, POP, and AS denote collections of photodiodes measuring at DC and radio frequencies (RFPDS).

Gravitational waves cause the arms of the interferometer to lengthen and contract relative to each other as the wave propagates through the detector. This changes the path length for light traveling in each arm, producing a relative phase difference detectable through interference. The fractional change in the length of the arms of the detector is known as strain and is proportional to the amplitude of the gravitational wave signal. Advanced LIGO's strain sensitivity curve is shown in figure 2. The black curve, which is a combination

of the individual noise sources shown in other colors, represents the minimum amplitude gravitational wave signal detectable in each frequency band.

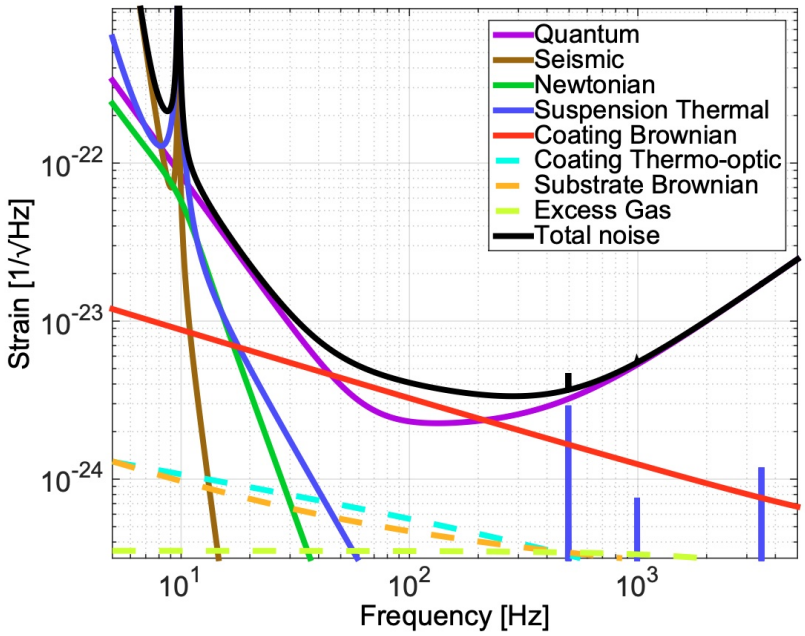

Figure 2: The sensitivity curve of Advanced LIGO [2]. Each line shows the amplitude spectral density of a noise source. The sum, in black, produces the predicted noise floor for advanced LIGO.

There are many length degrees of freedom (DoF) that must be controlled for the detector to operate. The most important of these is DARM, defined below.

$$L_- = \frac{L_x - L_y}{2} \tag{1}$$

For the detector to operate, these length DoFs need to be controlled. This is achieved by deriving error signals from sensors around the detector. These error signals drive feedback loops that keep the detector at its operating point. A block diagram of a simplified control loop for DARM is shown in figure 3. The plant of the control system is the suspension of the mirrors. These are disturbed by the gravitational wave signal and noise causing additional displacement to the mirrors. The sensors converts this to an error signal for DARM and the control block uses the error signal to drive actuators that apply force to the mirrors to return them to the set point. The DARM signal can calculated from the open loop transfer functions.

$$DARM = \frac{S}{1 - SPC}(n + g_w) \tag{2}$$

This length control system is needed to stabilize the detector against displacement noise to maintain a linear response to fluctuations in its DoF. However, by controlling mirror motion against displacements, the mirror motion due to gravitational wave signals is also suppressed. The gravitational wave signal is attained by applying the inverse of the closed loop transfer function from the displacement signal to DARM.

$$g_w = \frac{1 - \hat{S}\hat{P}\hat{C}}{\hat{S}} DARM \tag{3}$$

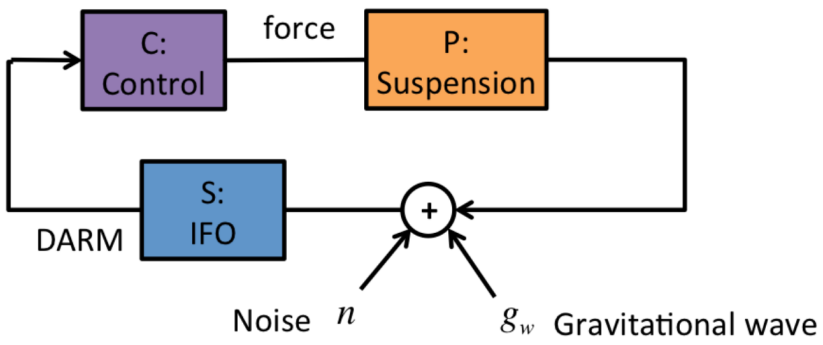

Figure 3: The control loop for DARM shown with the injection of displacement noise and gravitational wave signal [9].

The hats on the inverse transfer functions indicate that they are models that must be measured for accurate readout of the signal.

The control system is a key part of the detectors function. Currently, there are more sensors with some coupling to the length DoFs than there are length DoFs. A linear system that uses the outputs of all of these detectors would be overdetermined. The current control techniques only employ a subset of the sensors to generate a determined system: equal numbers of detectors and sensors. This project will explore the potential benefits to the sensitivity of the detector from designing an overdetermined control system that can take advantage of noise correlations between the detectors to reduce the susceptibility of the control system to various noise inputs.

2 PRMI Configuration

We consider the simplified detector configuration of a Michelson interferometer with a power recycling cavity(PRMI). This is a simplification of the Advanced LIGO detector configuration since there are no Faby-Perot cavities in the detector arms and no signal recycling mirror after the anti-symmetric port of the beam splitter to form a signal recycling cavity. There are two important length DoFs in this configuration, MICH and PRCL, defined in equations 4 and 5 respectively based on length definitions in figure 1. MICH is the difference in the arm lengths and PRCL is the length of the power recycling cavity.

$$l_- = \frac{l_x - l_y}{2} \tag{4}$$

$$l_p = l'_p + \frac{l_x + l_y}{2} \tag{5}$$

The 40m LIGO prototype at the California Institute of Technology is a 1:100 scale version of the Advanced LIGO detectors. These instrument is used for research and development of technologies for future gravitational wave detectors. This project will study the PRMI configuration of the 40m prototype.

3 40m LIGO prototype PRMI Length Control System

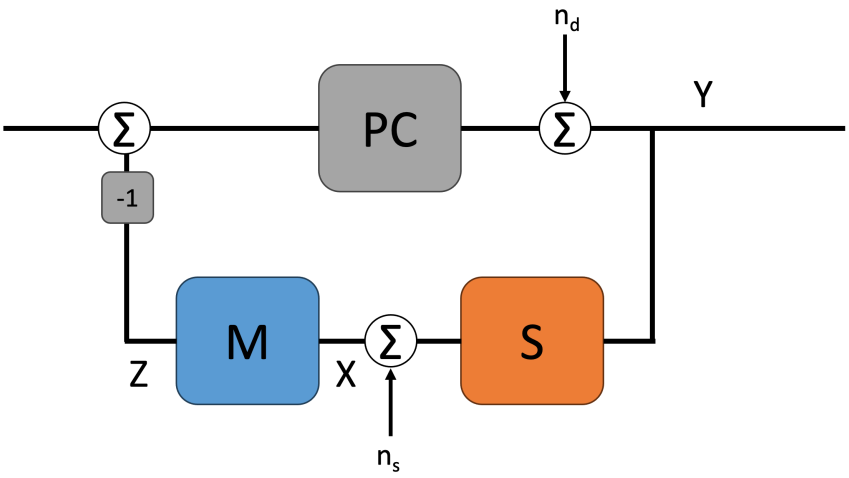

Figure 4: The block diagram for the control loop for MICH and PRCL in the PRMI configuration is shown.

A block diagram representing the general structure of the control system for MICH and PRCL is shown in figure 4. **PC** is the transfer function containing the control filters and the mechanical plant. Y is the state of MICH and PRCL. **S** is the Nx2 sensing matrix that maps MICH and PRCL states to N different sensors. **M** is the 2xN sensor fusion matrix which linearly combines the N sensors into 2 fused sensors. Displacement noise, n_d, cause fluctuations in MICH and PRCL that the need to be suppressed by controls. Sensing noise, n_s, represents all other noises that enter the loop due to the sensing and control process. This includes laser noise, ADC noise, photodiode dark noise, and other sources which can be correlated or uncorrelated between the detectors. The feedback system causes n_s to propagate to Y and become additional noise on MICH and PRCL. This is why care must be taken to generate the error signals for control. The current design of **M** selects one sensor for each DoF to generate an error signal and discards the rest of the sensors. Currently, PRCL is sensed with a REFL photodiode demodulated at 11MHz and MICH is sensed by an AS photodiode demodulated at 55 MHz.

4 PRMI LSC measurements

The 40m LIGO prototype was locked in the PRMI configuration by several of the LIGO lab staff. This allowed for open loop transfer functions for the MICH and PRCL control loops to be measured. These are shown in figure 5. 80 seconds of data was taken from 8 RF photodiodes, listed in table 1.

The amplitude spectral densities of the sensor signals are shown in 6. These signals will be calibrated into meters for multiple choices of **M** in later plots.

The sensing matrix was measured by driving MICH and PRCL with sinusoids at 211.1 Hz and 313.31 Hz respectively. The results are shown in table 2.

Table 1: A subset of the RFPDs used for the initial study of the PRMI LSC system are tabulated

Type	Demodulation frequency (MHz)	Demodulation phase (degrees)
AS	55	in-phase
AS	55	quadrature
REFL	55	in-phase
REFL	55	quadrature
REFL	11	in-phase
REFL	11	quadrature
REFL	165	in-phase
REFL	165	quadrature

Table 2: The the response of each detector to MICH and PRCL are shown. These elements form the sensing matrix.

Sensors	MICH (counts/meter)	PRCL (counts/meter)
AS55-I	$(+4.44 \pm 2.93)e+08$	$(+1.69 \pm 0.37)e+10$
AS55-Q	$(+9.89 \pm 1.00)e+09$	$(-3.77 \pm 0.50)e+09$
REFL55-I	$(-6.12 \pm 2.24)e+11$	$(+3.70 \pm 0.37)e+13$
REFL55-Q	$(+1.46 \pm 0.53)e+11$	$(-8.89 \pm 0.86)e+12$
REFL11-I	$(-1.43 \pm 0.53)e+10$	$(+9.13 \pm 0.86)e+11$
REFL11-Q	$(-7.73 \pm 3.71)e+08$	$(+5.13 \pm 0.50)e+10$
REFL165-I	$(-3.73 \pm 0.49)e+09$	$(+6.20 \pm 0.60)e+10$
REFL165-Q	$(-1.38 \pm 0.10)e+09$	$(-2.24 \pm 0.17)e+10$

5 Data Analysis

5.1 Relevant Transfer Functions

X can be calculated in terms of the injected noises.

$$X = (\mathbf{I} + \mathbf{SPCM}_0)^{-1} (\mathbf{S}n_d + n_s) \tag{6}$$

$$\mathbf{M}_0 = \begin{bmatrix} 0 & 1 & 0 & 0 & 0 & 0 & 0 & 0 \\ 0 & 0 & 0 & 0 & 1 & 0 & 0 & 0 \end{bmatrix} \tag{7}$$

$\mathbf{M}_0$ is the fusion matrix used during the PRMI lock that selects the AS55 quadrature-phase sensor for MICH and the REFL11 in-phase sensor for PRCL. The unsuppressed noises can be calculated from the sensor signals by transforming with $(\mathbf{I} + \mathbf{SPCM}_0.)$. The unsuppressed noise can be defined as follows.

$$X_{unsup.} = (\mathbf{I} + \mathbf{SPCM}_0)\, X \tag{8}$$

Then, the closed loop suppression of the feedback system with an alternative $\mathbf{M}$ can be calculated by mapping with $(\mathbf{I} + \mathbf{SPCM}.)^{-1}$. The simulated sensor signals X_{sim} is defined as follows.

$$X_{sim} = (\mathbf{I} + \mathbf{SPCM})^{-1} X_{unsup.} = (\mathbf{I} + \mathbf{SPCM})^{-1} (\mathbf{I} + \mathbf{SPCM}_0)\, X \tag{9}$$

The signal in the fused sensors can be calculated by mapping X_{sim} by $\mathbf{M}$.

$$Z_{sim} = \mathbf{M}X_{sim} = \mathbf{M}\,(\mathbf{I} + \mathbf{SPCM})^{-1} (\mathbf{I} + \mathbf{SPCM}_0)\, X \tag{10}$$

Finally, the simulated noises that would be measured on MICH and PRCL given $\mathbf{M}$ can be calculated from transforming Z_{sim} by $(\mathbf{MS})^{-1}$.

$$Y_{sim} = (\mathbf{MS})^{-1} Z_{sim} = (\mathbf{MS})^{-1}\mathbf{M}\,(\mathbf{I} + \mathbf{SPCM})^{-1} (\mathbf{I} + \mathbf{SPCM}_0)\, X \tag{11}$$

$\mathbf{M}$ and $\mathbf{S}$ are rectangular matrices so they do not have unique inverses, but their product, $\mathbf{MS}$, is a 2x2 matrix with a unique inverse that determines how the fused sensors relate to MICH and PRCL . An important consequence of this is that the $(\mathbf{MS})^{-1}\mathbf{M}$ factor in equation 8 does not simplify to cancel $\mathbf{M}$. We'll denote the complete transfer function from X to Y_{sim} as $\mathbf{G}_{X,Y_{sim}}$.

5.2 Power Spectral Densities of Frequency Domain Transformed Noise

The power spectral densities of the new signals derived from frequency domain transformation of the measured signals, X, are important for understanding performance of the sensor fusion matrices.

Suppose we have two frequency domain signal vectors $V(\omega)$ and $W(\omega)$ related by a transfer function $\mathbf{A}$.

$$V = \mathbf{A}W = \Sigma_i^N \Sigma_j^N a(\omega)_{ij} w(\omega)_j \tag{12}$$

The cross spectral density between between $v(\omega)_k$ and $v(\omega)_l$ can be calculated as follows.

$$CSD(v_k, v_l) = \lim_{T\to\infty} \frac{1}{T} v_k^* v_l = \lim_{T\to\infty} \frac{1}{T} \Sigma_i^N \Sigma_j^N (a(\omega)_{ki} w(\omega)_i)^* a(\omega)_{lj} w(\omega)_j \tag{13}$$

T is the time over which the signal is observed. We can exchange the order of the sum and the limit and factor $a(\omega)_{ki}^* a(\omega)_{lj}$ outside the limit since they have no dependence on T and we can assume that $CSD(x_i, x_j)$ is well defined for all i, j.

$$CSD(v_k, v_l) = \Sigma_i^N \Sigma_j^N a(\omega)_{ki}^* a(\omega)_{lj} \lim_{T\to\infty} \frac{1}{T} w(\omega)_i^* w(\omega)_j = \Sigma_i^N \Sigma_j^N a(\omega)_{ki}^* a(\omega)_{lj} CSD(w_i, w_j) \tag{14}$$

We can rewrite this last expression in a more concise form.

$$CSD(v_k, v_l) = \mathbf{A}_k \mathbf{CSD}(W) \mathbf{A}_l^H \tag{15}$$

$\mathbf{CSD}(W)$ refers to a matrix where the i, j element is $CSD(w_i, w_j)$ and $\mathbf{A}_i$ is column i of the transfer function matrix $\mathbf{A}$ and superscript H denotes hermitian conjugate. It follows that $\mathbf{CSD}(V)$ permits a simple expression in terms of $\mathbf{CSD}(W)$.

$$\mathbf{CSD}(V) = \mathbf{A}\mathbf{CSD}(W)\mathbf{A}^H \tag{16}$$

Therefore we can use the transfer functions calculated in the last section to transform $\mathbf{CSD}(X)$, the matrix of cross spectral densities of the sensors measured in the PRMI lock, to calculate the cross spectral density of the signals in the simulated control system. The main use of this is to calculate the simulated ASD of the MICH and PRCL with sensors fusion. This is calculated from the square root of the diagonal terms of $\mathbf{CSD}(Y_{sim})$.

$$\mathbf{CSD}(Y_{sim}) = \mathbf{G}_{X,Y_{sim}} \mathbf{CSD}(X) \mathbf{G}_{X,Y_{sim}}^H \tag{17}$$

6 Proposed Sensor Fusion Matrices and Simulated Results

6.1 Diagonalization

The current choice of sensor fusion matrix does not diagonalize $\mathbf{S}$.

$$\mathbf{M_0 S} = \begin{bmatrix} 9.89e+09 & -3.77e+09 \\ -1.43e+10 & 9.13e+11 \end{bmatrix} \tag{18}$$

The large off diagonal components result in cross coupling between MICH and PRCL. Therefore a simple potential improvement will be to choose the new sensor fusion matrix to diagonalize $\mathbf{S}$ and maintain the same on diagonal components.

$$\mathbf{MS} = \begin{bmatrix} 9.89e+09 & 0 \\ 0 & 9.13e+11 \end{bmatrix} \tag{19}$$

Since there are more sensors than DoFs, this condition does not uniquely specify **M**. A further improvement may be attained by specifying a cost function to optimize with respect to. This approach was taken to reduce the sensing noise entering the system at high frequencies.

6.2 High Frequency Sensing Noise Optimization

Above $\sim 10^3$Hz, the amplitude spectral densities of the sensor signals are white, reflecting that the signal composition is essentially only sensing noise. Therefore, $\mathbf{CSD}(X_{unsup})$ is a good approximation of the sensing noise injected into the system at high frequencies. This sensing noise enters the fused sensors, and the rest of the system, through **M**. Thus the cost function was derived from mapping $\mathbf{CSD}(X_{unsup})$ with **M**.

$$\mathbf{CSD}(Z_{n_s}) = \mathbf{M}\mathbf{CSD}(X_{unsup})\mathbf{M}^T \tag{20}$$

Each row of **M** defines the sensor fusion for one of the virtual sensors and so they can be optimized independently in this case. Thus the cost functions used to optimize the first row and second rows of **M** are the $\mathbf{CSD}(Z_{n_s})_{1,1}$ and $\mathbf{CSD}(Z_{n_s})_{2,2}$. These optimizations were done with respect to the constraint that **M** diagonalize **S** as described

6.3 Results

The simulated amplitude spectral densities of MICH and PRCL are shown in figure 8. The open loop noises on MICH and PRCL were calculated by mapping $\mathbf{CSD}(X_{unsup.})$ by $\mathbf{S}^+$, the Moore-Penrose inverse of the sensing matrix. The data for the current sensor fusion matrix is shown in orange, the **M** chosen to diagonalize **S** is used for the green curve, and the high frequency optimized sensor fusion matrix is shown in red. For both MICH and PRCL, the new sensor fusion techniques show improvement in certain frequency bands. Both techniques show improvement at low frequencies by removing cross coupling between DoFs and the noise optimized **M** does indeed show reduced sensing noise at high frequencies.

7 Summary and Next Steps

Methods have been developed to use measurements of the PRMI length sensing and control system to predict the performance of the loop as a function of the sensor fusion matrix **M**. Two techniques for calculating **M** have been suggested and they are both predicted to reduce the amplitude spectral density of noise on both MICH and PRCL over a range of frequencies. These techniques should be evaluated on the 40m LIGO prototype by implementing the new sensor fusion techniques during a PRMI lock and measuring the resulting noise ASDs. In addition, new cost functions can be explored to optimize the **M** over different frequency ranges and with more sophisticated techniques to estimate the sensing noise.

References

[1] B. P. Abbot et al. (LIGO Scientific Collaboration and Virgo Collaboration). Observation of Gravitational Waves from a Binary Black Hole Merger. Phys. Rev. Lett., 116, 061102 (2016).

[2] L. Barsotti, S. Gras, M. Evans, P. Fritschel. The updated Advanced LIGO design curve. (2018)

[3] Aasi, J., Abadie, J., Abbott, B. et al. Enhanced sensitivity of the LIGO gravitational wave detector by using squeezed states of light. Nature Photon. 7, 613-619 (2013).

[4] LIGO Scientific Collaboration. Advanced LIGO. arXiv:1411.4547 (2014).

[5] Gilbert Grynberg, Alain Aspect, and Claude Fabre. Introduction to Quantum Optics. Chapter 5 (2010).

[6] Mark Fox. Quantum Optics An Introduction. Chapter 7 (2006).

[7] G. Venugopalan et al. Prototype Interferometry in the Era of Gravitational Wave Astronomy, Phys. Rev. A, 102, 023507 (2020)

[8] E. A. Quintero et al. Improving the Performance and Sensitivity of Gravitational Wave Detectors. Review of Scientific Instruments, 87, 065107 (2016)

[9] Brett Shapiro. Intro to Control Theory for LIGO People. Lecture 2, G1600726-v3.

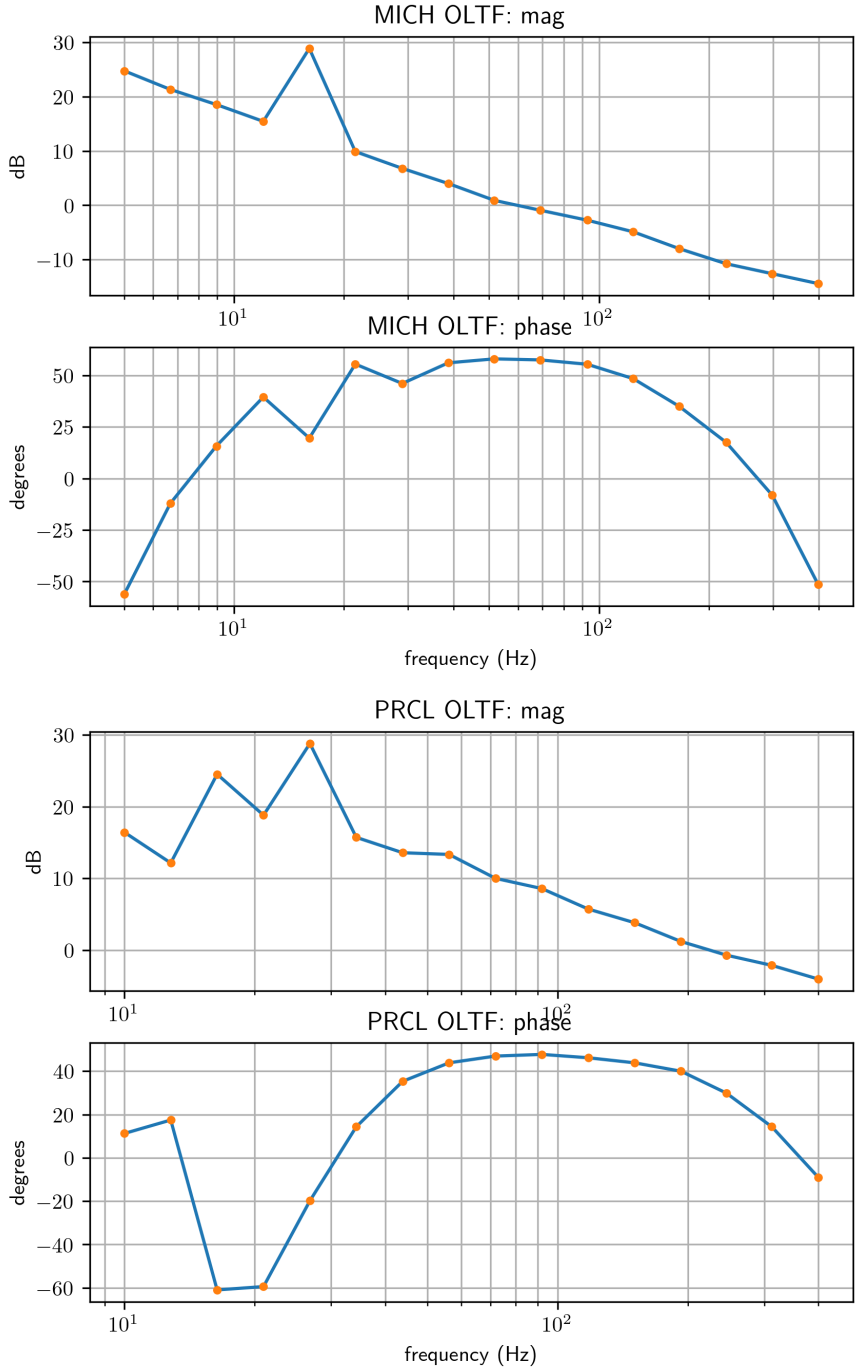

Figure 5: The open loop transfer functions for MICH and PRCL during the PRMI lock are shown. The coherence of the PRCL OLTF was poor below 60 Hz so the gain and phase were extrapolated from higher frequencies.

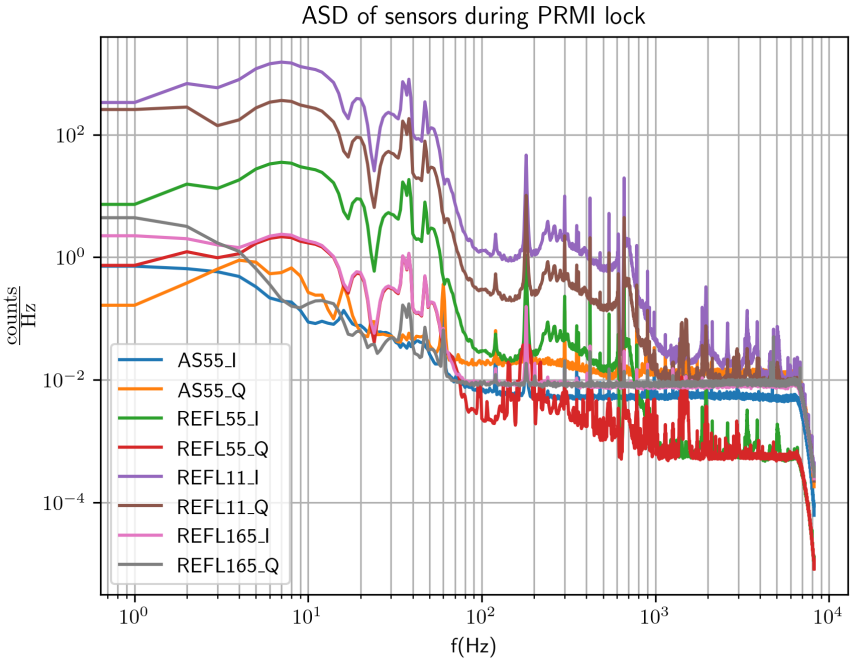

Figure 6: The amplitude spectral density of the sensors signals during the PRMI lock are shown.

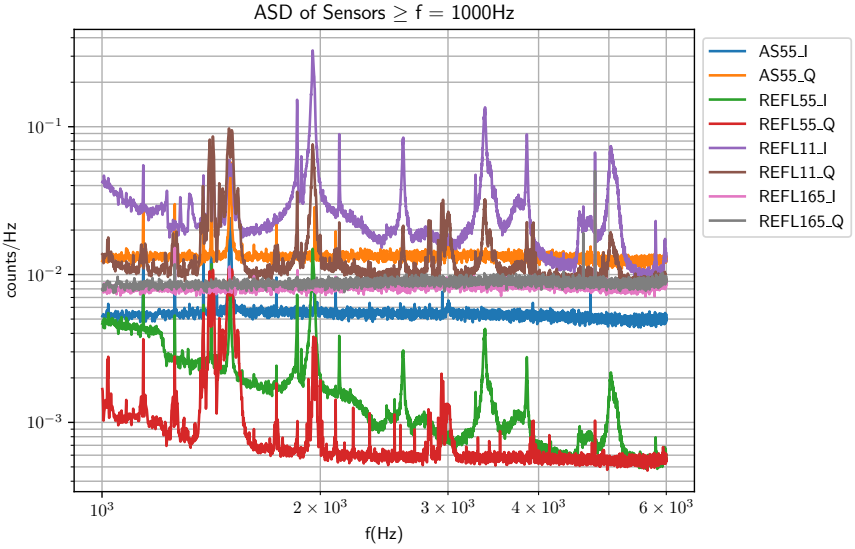

Figure 7: The ASD of the sensor data above 1KHz.

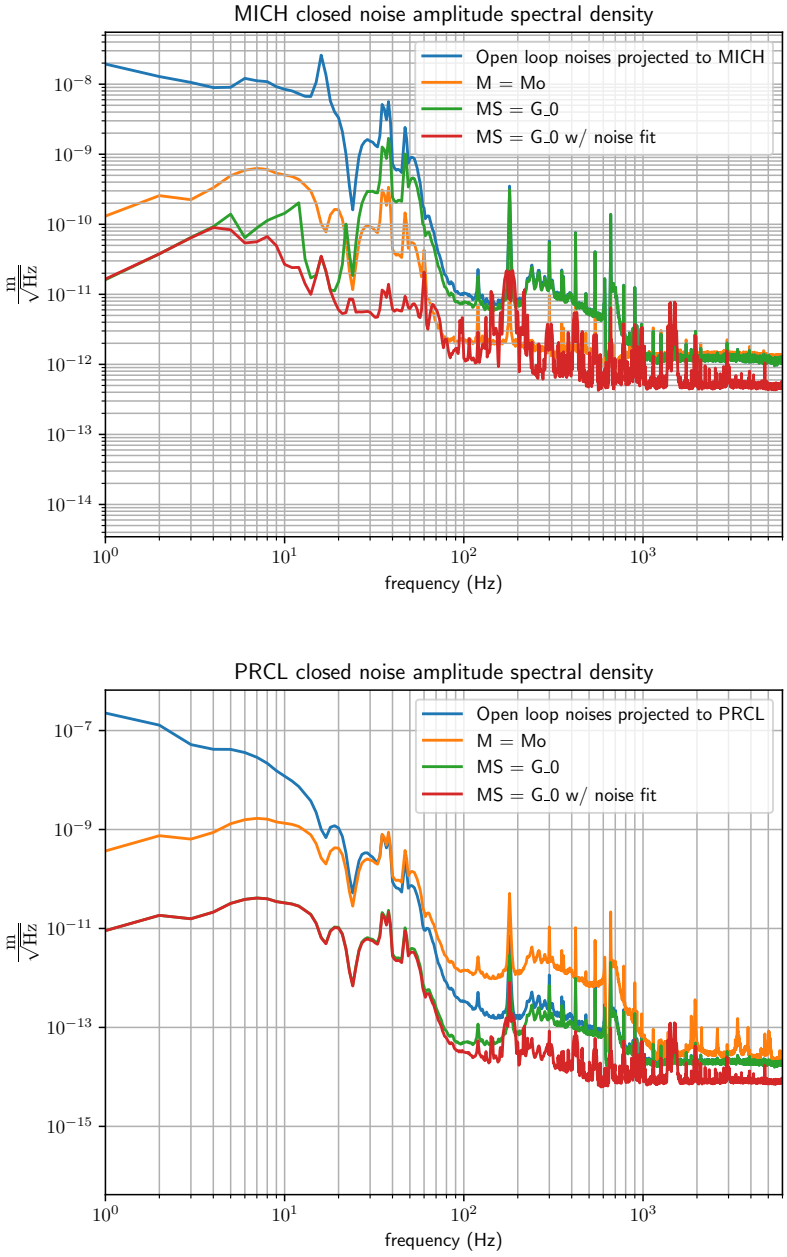

Figure 8: The ASD of the simulated noises on MICH and PRCL for several choices of **M**.